APS physics

CHORUS

This is the accepted manuscript made available via CHORUS. The article has been published as:

Measurements of the generalized electric and magnetic polarizabilities of the proton at low Q^{2} using the virtual Compton scattering reaction

P. Bourgeois *et al.*

Phys. Rev. C **84**, 035206 — Published 29 September 2011

DOI: 10.1103/PhysRevC.84.035206

Measurements of the Generalized Electric and Magnetic Polarizabilities of the Proton at Low Q^2 Using the VCS Reaction

P. Bourgeois,[1] Y. Sato,[2] J. Shaw,[1] R. Alarcon,[3] A. M. Bernstein,[4] W. Bertozzi,[4] T. Botto,[4] J. Calarco,[5] F. Casagrande,[4] M. O. Distler,[6] K. Dow,[4] M. Farkondeh,[4] S. Georgakopoulos,[7] S. Gilad,[4] R. Hicks,[1] M. Holtrop,[5] A. Hotta,[1] X. Jiang,[8] A. Karabarbounis,[7] J. Kirkpatrick,[5] S. Kowalski,[4] R. Milner,[4] R. Miskimen,[1] I. Nakagawa,[4,*] C. N. Papanicolas,[7] A. J. Sarty,[9] S. Sirca,[4] E. Six,[3] N. F. Sparveris,[7] S. Stave,[4] E. Stiliaris,[7] T. Tamae,[2] G. Tsentalovich,[4] C. Tschalaer,[4] W. Turchinetz,[4] Z.-L. Zhou,[4] and T. Zwart[4]

[1]Department of Physics, University of Massachusetts, Amherst, Massachusetts 01003 USA

[2]Laboratory of Nuclear Science, Tohoku University , Mikamine, Taihaku, Sendai 982-0826 Japan

[3]Department of Physics and Astronomy, Arizona State University, Tempe, Arizona 85287, USA

[4]Department of Physics, Laboratory for Nuclear Science and Bates Linear Accelerator Center, Massachusetts Institute of Technology, Cambridge, Massachusetts 02139, USA

[5]Department of Physics, University of New Hampshire, Durham, New Hampshire 03824, USA

[6]Institute fur Kernphysik, Universitaet Mainz, Mainz, Germany

[7]Institute of Accelerating Systems and Applications and Department of Physics, University of Athens, Athens, Greece

[8]Los Alamos National Laboratory, Los Alamos,, New Mexico

[9]Department of Astronomy and Physics, St. Mary's University, Halifax, Nova Scotia, Canada

Experimental details of a virtual Compton scattering (VCS) experiment performed on the proton at the MIT-Bates out-of-plane scattering facility are presented. The VCS response functions $P_{LL} - P_{TT}/\varepsilon$ and P_{LT} have been measured at $Q^2 = 0.057\,GeV^2/c^2$. The generalized electric and magnetic polarizabilities, $\alpha(Q^2)$ and, $\beta(Q^2)$ and the mean square electric polarizability radius, $\langle r_\alpha^2 \rangle$, are obtained from a dispersion analysis of the data. The results are in good agreement with $O(p^3)$ heavy baryon chiral perturbation, and indicating the dominance of mesonic effects in the polarizabilities.

PACS numbers: 13.60.Fz, 14.20.Dh, 13.40.Gp, 13.40.-f,

1. Introduction

The topic of hadron polarizabilities has generated considerable theoretical and experimental interest [1]. Although the electric and magnetic polarizabilities of the proton, α and β, are known with reasonable accuracy from real Compton scattering (RCS) [2], very little is known about the distribution of polarizability density inside the nucleon. The dominant pion loop diagrams for the proton polarizability and the proton E.M. form factor are shown in Fig. 1. The presence of an additional electromagnetic vertex in the polarizability diagram relative to the form factor diagram implies that the proton polarizability distribution will not be identical to the proton charge distribution. To measure a polarizability density it is necessary to use the virtual Compton scattering (VCS) reaction [3], where the incident photon is virtual.

At low Q^2 it has long been assumed [4] that the generalized electric polarizability, $\alpha(Q^2)$, should decrease monotonically with increasing Q^2 with a length scale given by the pion range, where Q^2 is the 4-momentum transfer to the nucleon. By contrast, most theoretical predictions for the generalized magnetic polarizability predict that $\beta(Q^2)$ should rise with increasing Q^2, and then decrease. The cancellation of negative long-range diamagnetism of the proton, due to the pion cloud, with the positive short-distance paramagnetism of the proton, due to the quark core, causes the predicted peaked behaviour for $\beta(Q^2)$.

RCS [2] and VCS experiments at Mainz [5] and JLab [6] did establish that $\alpha(Q^2)$ is falling off with increasing Q^2, and that $\beta(Q^2)$ is relatively flat at low Q^2. However, the Mainz data [5] and more recent data from Bates [7] at $Q^2 = 0.057\,GeV^2$ suggests there is a peaking of $\alpha(Q^2)$ in the region of $Q^2 = 0.3GeV^2$, a trend confirmed by new data from Mainz [8] at $Q^2 = 0.33GeV^2$ In this paper the experimental details of a VCS experiment [7] performed on the proton using the out-of-plane scattering facility at the MIT-Bates Linear Accelerator are presented. The data were taken at sufficiently

low $Q^2 = 0.057 GeV^2$ that the data have sensitivity to the mean square electric polarizability radius of the proton, as well as providing a test of chiral perturbation theory.

2. The VCS reaction

The relationship between VCS cross sections and the polarizabilities is most easily seen in the low energy expansion (LEX) of the unpolarized VCS cross section [3]

$$d^5\sigma^{VCS} = d^5\sigma^{BH+Born} + q'\Phi\Psi_0(q,\varepsilon,\theta,\phi) + O(q'^2) \quad (1)$$

where $q(q')$ is the incident (final) photon 3-momenta in the photon-nucleon C.M. frame, ε is the photon polarization, $\theta(\phi)$ is the C.M. polar (azimuthal) angle for the outgoing photon, and Φ is a phase space factor. $d^5\sigma^{BH+Born}$ is the cross section for the Bethe-Heitler + Born amplitudes only, i.e. no nucleon structure, and is exactly calculable from QED and the nucleon form factors. The Bethe-Heitler and Born diagrams for the VCS reaction are shown in Fig. 2. The polarizabilities enter the cross section expansion at order $O(q')$ through the term Ψ_0, given by [9]

$$\Psi_0(q,\varepsilon,\theta,\phi) = V_1\left[P_{LL}(q) - \frac{P_{TT}(q)}{\varepsilon}\right] + V_2 P_{LT}(q) \quad (2)$$

where $P_{LL}(q)$, $P_{TT}(q)$, and $P_{LT}(q)$ are VCS response functions. The response function $P_{LL}(q)$ is proportional to $\alpha(Q^2)$, $P_{LT}(q)$ is proportional to $\beta(Q^2)$ + spin-polarizability term, and $P_{TT}(q)$ is proportional to spin-polarizability terms. The terms V_1 and V_2 are kinematic functions. The Bates VCS experiment was designed to make an azimuthal separation of $P_{LL} - P_{TT}/\varepsilon$ and P_{LT} by taking data simultaneously at $\theta = 90°$ at the azimuthal angles $\phi = 90$, 180 and 270 degrees. At fixed θ the VCS cross sections at $\phi = 90°$ and $270°$ are equal and the kinematic function V_2 goes to zero. Therefore, the polarizability effect Ψ_0 is proportional to $P_{LL} - P_{TT}/\varepsilon$. At $\varphi = 180°$ both V_1 and V_2 are non-zero, and the polarizability effect is proportional to a weighted sum of $P_{LL} - P_{TT}/\varepsilon$ and P_{LT}. All of the data were taken with $q = 240$ MeV/c, and $\varepsilon = 0.9$, which corresponds to $Q^2 = 0.057 GeV^2$. At these kinematics the percentage of $P_{LL} - P_{TT}/\varepsilon$ that comes from $\alpha(Q^2)$ is estimated [4] at 92%, with the

remainder coming from the spin-polarizabilities. The percentage of P_{LT} that comes from $\beta(Q^2)$ is estimated [4] at 69%, with the remainder coming from the spin-polarizabilities. Table 1 lists the incident beam energies and the corresponding C.M. final photon energies in the experiment. At $q' = 43$ MeV/c the polarizability effect is negligible in the cross sections, and at $q' = 115$ MeV/c the polarizability effect is approximately 20%.

3. The MIT-Bates VCS experiment

This experiment was the first to use extracted high duty-factor beam from the MIT-Bates South Hall Ring. The extracted beams had duty factors of approximately 50%, with currents up to 7 μA. The target was a closed circulating loop of liquid hydrogen, where the liquid hydrogen circulated vertically in a 1.6 cm diameter tube through the electron beam spot. The target cell wall was 4.3 μm thick havar in the region where the beam passed through the target cell wall.

The full Out-of-Plane Spectrometer (OOPS) system with gantry was used for proton detection [10]. The OOPS proton detection system consists of four identical vertically bending dipole-quadrupole spectrometers. The gantry support system allows one OOPS to be positioned above the scattering plane and another OOPS to be positioned below the scattering plane. An additional OOPS was positioned in the scattering plane using a satellite support system. The standard drift distance from the target to the OOPS is 1.4 m. A new OOPS optics tune using a 2.5 m drift distance was developed for running at final photon energies $q' = 43$ and $q' = 65$ MeV/c because the OOPS were at angles so close together that they would mechanically interfere with each other at the shorter drift distance. Data taken at higher q' used the standard 1.4 m drift for the OOPS.

The standard OOPS trigger is a three-fold coincidence of three plastic scintillators in the OOPS focal plane, where the scintillators have thicknesses of 0.16 cm, 0.48 cm, and 0.48 cm. Since the lowest proton kinetic energy in the experiment was 30 MeV, there was concern that the protons might stop in the first two trigger scintillators, and for this reason, the OOPS trigger was modified to a coincidence of the first two scintillators in the OOPS focal plane. A GEANT simulation of the OOPS trigger predicts a trigger efficiency of approximately 99%.

The OHIPS electron spectrometer used a new focal plane [11] that increased the momentum acceptance of the spectrometer from 9% to 13%, which served to increase the acceptance in q'. Beam-optics studies were performed to measure OHIPS transport matrix elements over the extended focal plane instrumentation. A montecarlo based on the program Turtle [12] was used to calculate acceptance. The montecarlo utilized spectrometer matrix elements from the beam-optics studies, and the multiple scattering model [13] from GEANT4. Good agreement was achieved between measured and calculated angular and momentum distributions.

The final state photon in the reaction was identified through missing mass and time-of-flight techniques. Because the duty factor of the beam was less than 100%, the experimental time-of-flight (TOF) distribution shown in Fig. 3 panel (a) does not exhibit the flat accidental distribution typically observed at high-duty factor facilities such as Jefferson Laboratory or MAMI at Mainz; in this case accidentals peak under the coincidence peak. The first step in the analysis was to make an approximate subtraction of accidentals by cutting on the coincident peak in the TOF distribution. The coincident and accidental missing mass squared (MM^2) distributions are shown in Figs. 3-b and 3-c, respectively. The result of subtracting the accidental MM^2 distribution from the coincident MM^2 distribution is shown in Fig. 3-d, where the subtraction weighting factor is given by the timing widths of the accidental and coincident TOF bins. The subtraction of accidentals at this stage is only approximate because the accidental events are peaked in the TOF distribution. The peak in the subtracted MM^2 distribution, shown in Fig. 3-d, contains the coincident VCS events, and the background under this peak contains unsubtracted accidentals and coincident $A(e,e'p)X$ events on the havar target cell wall. Empty target runs were not taken because electron beam heating would have caused damage to the target cell wall. Photon yields were obtained by fitting the subtracted MM^2 distributions using a radiated, real-photon line shape calculated with the montecarlo, and an empirical background shape that accounts for both the unsubtracted accidentals and coincident target background events. Polynomial and skewed Gaussian shapes for the background gave identical yields within errors to a fit that used the accidental MM^2 distribution (see Fig. 3-c) for the background shape. For simplicity, the accidental MM^2 distribution was utilized for background fitting in

the subtracted MM^2 distribution, and Fig. 3-d shows a typical fit. Photon yields were obtained by subtracting the fitted background distribution from the accidentals subtracted MM^2 distribution, and then summing counts over the real photon peak. Radiative corrections were applied to the data [14], approximately 22% in these kinematics.

The VCS cross sections are shown in Fig. 4 with the statistical and systematic errors combined in quadrature. The dominant errors are statistical for all of the VCS cross sections. The largest systematic errors in the cross sections are the OOPS tracking efficiency and the luminosity measurement, and these errors are presented in Table 2. The OOPS tracking efficiency is measured by taking the ratio of events with a good track in the OOPS drift chambers to the number of OOPS trigger events. The uncertainty in the tracking efficiency results from the statistical errors in these numbers. The luminosity measurement was limited primarily by uncertainties in subtracting pedestal charge from the measured Faraday Cup charge. The systematic error in the luminosity was estimated by calculating the ratio of the measured charge to the number of electron singles events in OHIPS for each data production run of approximate duration one hour. The standard distribution of the mean of these ratios over each VCS data set was taken as the uncertainty in the luminosity. Uncertainty in the incident beam energies, estimated at $\pm 0.1\%$ [15], introduces an uncertainty in the response functions and polarizabilities through the beam energy dependence of $d^5\sigma^{BH+Born}$. The fractional variation in $d^5\sigma^{BH+Born}$ due to the beam energy uncertainty, presented in Table 2, is comparable to the OOPS tracking efficiency uncertainty. The cross sections with statistical and systematic errors are presented in Table 3.

4. Low-Energy-Expansion Analysis of the data

An analysis of the data was performed using the low-energy expansion (see Eq. 1). The dotted lines in Fig. 4 are the Bethe-Heitler+Born (BH+Born) calculations, i.e. no polarizability effect, using Hoehler form factors [16]. The agreement between data and the BH+Born calculation is good at low q', while at higher q' the out-of-plane data falls significantly below the calculation because of the destructive interference between the BH+Born and polarizability amplitudes. The in-plane cross sections show a much smaller deviation from the BH+Born cross sections at high q'. This smaller deviation from the BH+Born

for the in-plane cross sections results from V_1 and V_2 in Eq. (2) having the same sign, and $P_{LL} - P_{TT}/\varepsilon$ positive and P_{LT} negative. Therefore the charge and magnetic polarizabilities interfere destructively at $O(q')$ for the in-plane cross sections. Because of this cancellation the LEX analysis of the in-plane data for P_{LT} will not be reliable, and it will be necessary to use a dispersive analysis that includes all orders in q'.

The dashed lines in Fig. 4 are fits to the cross section data using the LEX analysis, i.e. Eqn. (1). These fits give $P_{LL} - P_{TT}/\varepsilon = 54.5 \pm 4.8 \pm 3.4 GeV^{-2}$, and $P_{LT} = -20.4 \pm 2.9 \pm 1.4 GeV^{-2}$, with the first error statistical and the second error systematic. Systematic errors were propagated into the LEX analysis using a montecarlo technique, where the parameters in Table 2 are randomly varied within their limits, and the incident beam energy at each q' setting was varied within an uncertainty of ±0.1%. A LEX analysis was performed at each variation of parameters, the parameter variation and data fitting being repeated thousands of times. The standard deviations of the resulting distributions for $P_{LL} - P_{TT}/\varepsilon$ and P_{LT} were taken as the systematic errors in the response functions. A LEX analysis using the Friedrich-Walcher form factors [17] gives identical results, within errors, to the analysis presented here using the Hoehler form factors

The LEX result for $P_{LL} - P_{TT}/\varepsilon$ is shown in Fig. 5 along with results from Mainz and Jefferson Lab, where the statistical and systematic errors have been combined in quadrature. Also shown in the figure is the parameter free $O(p^3)$ calculation in heavy baryon chiral perturbation theory (HBChPT) [4], which is in good agreement with experiment for $P_{LL} - P_{TT}/\varepsilon$. The LEX result for P_{LT} is not shown in Fig. 5 because of the cancellation of the polarizability effect at $O(q')$ for the in-plane cross sections, which makes necessary a dispersive approach to extracting P_{LT} from the data.

5. Dispersion Analysis of the Data

A dispersion analysis of the data was performed using the VCS dispersion model [18]. The VCS amplitudes are obtained from the MAID $\gamma^* p \to \pi N$ multipoles [19], and unconstrained asymptotic

contributions to 2 of the 12 VCS amplitudes. For fitting VCS data a dipole anstatz has traditionally been used [18] to parameterize the asymptotic contributions,

$$\alpha(Q^2) - \alpha^{\pi N}(Q^2) = \frac{\alpha^{\exp} - \alpha^{\pi N}}{(1 + Q^2/\Lambda_\alpha^2)^2} \tag{3}$$

with a similar parameterization defined for $\beta(Q^2)$. In this equation $\alpha^{\exp}$ is the experimental electric polarizability from RCS, $\alpha^{\pi N}$ in the calculated πN contribution to the electric polarizability at $Q^2 = 0$, and $\alpha^{\pi N}(Q^2)$ is the calculated πN contribution to the electric polarizability at the experimental Q^2. The only free parameter in Eqn. 3 is Λ_α. It is important to note that there is no loss of generality by using the dipole parameterization of Eqn. 3, and any Q^2 parameterization can be used. The parameters Λ_α and Λ_β are fit to the experimental cross sections at one Q^2 point, and the solid curves in Fig. 4 show the best dispersion fits to the VCS cross sections. Once Λ_α and Λ_β have been fit to the data, the polarizabilities $\alpha(Q^2)$ and $\beta(Q^2)$ are obtained from Eqn. 3, and its generalization for the magnetic polarizability. The response functions $P_{LL} - P_{TT}/\varepsilon$ and P_{LT} are found by summing the asymptotic terms with calculated πN dispersive contributions.

The best fit response functions from the dispersion analysis are $P_{LL} - P_{TT}/\varepsilon = 46.7 \pm 4.9 \pm 3.4 GeV^{-2}$ and $\mathrm{P_{LT}} = -8.9 \pm 4.2 \pm 1.4 \mathrm{GeV}^{-2}$, where the first error is statistical and the second is systematic. Since the sensitivities of the response functions to the systematic errors are approximately the same for the dispersion and LEX analyses, the systematic errors for the dispersion analysis are taken from the LEX monte carlo analysis. The fitted values for Λ_α and Λ_β are given in table 4, along with results from the Jefferson Lab dispersion analysis. The Jefferson Lab 1-a analysis utilizes data taken below pion threshold, and the 1-b analysis utilizes data taken between one and two pion threshold.

An alternate fitting procedure was also applied to obtain Λ_α and Λ_β, where simulated events are distributed within the experimental acceptance using event weighting given by the dispersion analysis cross

sections. The number of accepted simulation events are compared with the experimental number of counts, and then Λ_α and Λ_β are varied to minimize chi-squared. The values of Λ_α and Λ_β obtained from the count based analysis, $0.53 \pm^{0.13}_{0.08}$ and $0.41 \pm^{0.22}_{0.12}$, respectively, agree within errors with the cross section based analysis.

The dispersion results for $P_{LL} - P_{TT} / \varepsilon$ and P_{LT} are shown in Fig. 5 with the statistical and systematic errors combined in quadrature. The figure shows that the dispersion result for $P_{LL} - P_{TT} / \varepsilon$ is in near agreement with the LEX analysis and the HBChPT predictions. The dispersion result for P_{LT} is also in good agreement with the HBChPT prediction.

The dashed curves in Fig. 5 are the dispersion model calculations for $P_{LL} - P_{TT} / \varepsilon$ and P_{LT} assuming the dipole choice of Eqn. 3 and fitted values of Λ_α and Λ_β . By construction, the dispersion calculations go directly through the RCS and MIT-Bates data points. For P_{LT} , there is relatively good agreement between the dispersion calculation and the JLab 1-a, 1-b, and Mainz data points. Based on this comparison, the dipole anstatz of Eqn. 3 appears to be a good approximation for representing $\beta(Q^2)$. Further evidence for this is seen in the Λ_β fit values shown in table 4, where the MIT-Bates and JLab results agree within their statistical and systematic errors. For $P_{LL} - P_{TT} / \varepsilon$ there is also relatively good agreement between the dispersion calculation and the JLab 1-a and 1-b data points; the fitted Λ_α values from MIT-Bates and JLab are in agreement. However, there is a significant gap between the dispersion calculation for $P_{LL} - P_{TT} / \varepsilon$ and the Mainz data points, indicating that the dipole assumption of Eqn. 3 is a poor approximation in this intermediate Q^2 range.

The spatial dependence of the induced polarization in an external electromagnetic field has recently been calculated in the light-front frame [20]. By adding a Gaussian to the asymptotic term in Eqn. 3 for $\alpha(Q^2)$, the authors of [20] were able to obtain a good fit to the experimental data for $P_{LL} - P_{TT} / \varepsilon$. The calculation of the induced polarization in a proton with definite light-cone helicity shows that without the Gaussian asymptotic term, the induced polarization becomes small at distances

beyond 0.5 fm, whereas with the Gaussian term there is a pronounced structure in the induced polarization at transverse distances of 0.5 to 1 fm.

The dispersion model fit of the MIT-Bates data gives $\alpha = (7.85 \pm 0.87 \pm 0.60) \times 10^{-4}\, fm^3$, and $\beta = (2.69 \pm 1.48 \pm 0.49) \times 10^{-4}\, fm^3$. These results are shown in Figs. 6a and 6b with the statistical and systematic errors combined in quadrature, along with previous results from RCS [2], Mainz [21] and JLab [6]. The MIT-Bates results for α and β are in near agreement with the HBChPT prediction, shown as the solid curves in Figs. 6a and 6b. The theoretical errors for the HBChPT calculation of $\alpha(Q^2)$ and $\beta(Q^2)$ at $Q^2 = 0.06 GeV^2$ are estimated [22] to be comparable to the errors for an $O(p^4)$ calculation [23] of α and β, approximately ± 2.0 and ± 3.6 in units of $10^{-4}\, fm^3$, respectively.

A fully dispersive analysis of the Mainz data [5] [8] for α and β is in progress, but not published [21], and the "Mainz 2000" points shown in Figs. 6a and 6b are actually derived from a LEX analysis of the first Mainz VCS experiment [5]. In that analysis the proton spin-polarizabilities were calculated using dispersion theory, and the spin-polarizability contributions were subtracted from the LEX response functions [21]. We performed a similar analysis using the new Mainz response functions [8], and the polarizabilities obtained are $\alpha = 8.22 \pm 0.62 \pm 0.98 \times 10^{-4}\, fm^3$ and $\beta = 3.55 \pm 0.37 \pm 1.15 \times 10^{-4}\, fm^3$. These results are shown in Figs. 6a and 6b as "Mainz 2008" data points.

The dashed curve in Figs. 6a and 6b is a dispersion model calculation using the same Λ_α and Λ_β parameters as the calculation shown in Fig. 5. The dotted and dash-dotted curves are the πN and asymptotic contributions to the polarizabilities, respectively. Fig. 6b shows that the πN term from the $\Delta(1232)$ resonance is paramagnetic (positive), whereas the asymptotic contribution is diamagnetic (negative). The dispersion calculation for α falls significantly below the Mainz data points at $Q^2 = 0.33 GeV^2/c^2$, while the dispersion calculation for β is in relatively good agreement with the Mainz and JLab I-a data points.

6. *Mean-square polarizability radii*

The mean square electric polarizability radius $\left\langle r_\alpha^2 \right\rangle$ is given by,

$$\left\langle \mathrm{r}_\alpha^2 \right\rangle = \frac{-6\hbar^2}{\alpha^{\exp}} \frac{\mathrm{d}}{\mathrm{dQ}^2} \alpha\left(\mathrm{Q}^2\right)\Big|_{\mathrm{Q}^2=0} \tag{4}$$

$\left\langle r_\alpha^2 \right\rangle$ was determined using the dispersion analysis fit to the experimental data, where $\alpha(\mathrm{Q}^2)$ is given by Eqn. 3., with Λ_α fixed by the fit to the experimental data, and $\alpha^{\pi N}(Q^2)$ given by the dispersion calculation. Evaluating Eqn. 4 using the functional form of $\alpha(\mathrm{Q}^2)$ given by Eqn. 3 gives $\left\langle r_\alpha^2 \right\rangle = 2.02^{+0.39}_{-0.59}\, fm^2$, which is in good agreement with the HBChPT prediction [24] of $1.7\, fm^2$. The error is statistical only. The experimental value is significantly larger than the proton mean square charge radius [25] of $0.757 \pm .014\, fm^2$, showing that mesonic effects are the dominant effect in describing the electric polarizability. It is interesting to note that the experimental mean-square radius is in good agreement with an uncertainty principle estimate for the size of the pion cloud, $< \mathrm{r}^2 > \approx \left(\hbar \mathrm{c}/\mathrm{m}_\pi\right)^2 = 2\mathrm{fm}^2$. The dominant pion loop diagrams for the proton form factor and the proton polarizability are shown in Fig. 1. The additional electromagnetic vertex in the polarizability diagram relative to the form factor diagram serves to increase the range of the interaction by approximately 70% as compared to the charge form factor.

Mean-square electric and magnetic polarizability radii are presented in Table 5. Also shown in the table are mean-square radii for the πN and asymptotic contributions to the polarizabilities. Because the error on the MIT-Bates $\beta(\mathrm{Q}^2)$ is large compared to $\beta^{\exp}$, the data doesn't place a useful constraint on $\left\langle \mathrm{r}_\beta^2 \right\rangle$. The mean-square radii for the asymptotic and πN contributions to $\alpha(Q^2)$ are approximately equal, and are close to $1.0\mathrm{fm}^2$. Although errors in the mean-square radii for the asymptotic (diamagnetic) and πN (paramagnetic) contributions to $\beta(\mathrm{Q}^2)$ are relatively large, there is a suggestion in the data that

the diamagnetic mean-square radius is larger than the paramagnetic mean-square radius, which supports a conceptual view of the proton as having long-range diamagnetism, due to the pion cloud, and short-distance paramagnetism, due to the quark core.

7. Summary and conclusions

The experimental results are summarized in Table 6. Because of the cancellation of the polarizability effect at $O(q')$ for the in-plane cross sections, the LEX result for P_{LT} is not shown in Table 6. The MIT-Bates VCS experiment supports two strongly held concepts about the proton polarizability. The first is that the electric polarizability is dominated by mesonic effects. This is confirmed by the large size of $\langle r_\alpha^2 \rangle$ relative to the proton charge radius. The second is the cancellation of paramagnetism by diamagnetism in the proton, a conjecture that is critical in all explanations of the small size of β relative to α, since in HBChPT the sizes of the polarizabilities are predicted to be of the same order. Because paramagnetism from the $\Delta(1232)$ resonance is predicted to be nearly independent of Q^2 in this low Q^2 range, the predicted paramagnetic-diamagnetic interference will also have a relatively flat dependence on Q^2. The data does indicate that $\beta(Q^2)$ is relatively flat as a function of Q^2, in agreement with the HBChPT prediction.

The data for $P_{LL} - P_{TT}/\varepsilon$ and $\alpha(Q^2)$ show that $\alpha(Q^2)$ does not have a monotonic, dipole-like dependence over the Q^2 interval from 0.05 to 1 GeV^2. This is a wholly unanticipated discovery, at odds with what has long been known about the Q^2 behavior of the proton charge and magnetic form factors. A fit to the data for $P_{LL} - P_{TT}/\varepsilon$ using a light-front calculation [20] indicates that there is pronounced structure in the induced polarization at transverse distances of 0.5 to 1 fm, whereas the traditional dipole anstatz of Eqn. 3 gives no structure at transverse distances beyond 0.5 fm.

With the closing of the MIT-Bates Linear Accelerator for experimental nuclear physics, the Mainz accelerator is the only remaining facility world-wide that is suitable for VCS studies at low to medium

Q^2 . A new program of studies at Mainz to measure the unpolarized VCS response functions $P_{LL} - P_{TT}/\varepsilon$ and P_{LT} over the interval from $Q^2 = 0.1$ to 0.5 GeV^2 will be essential to pin down the behavior of $\alpha(Q^2)$ and $\beta(Q^2)$ in this interesting region.

TABLE 1. VCS kinematics. $E_i(E_f)$ is the incident(final) electron energy in MeV, θ_e is the laboratory electron scattering angle in degrees, and $q(q')$ is the incident(final) photon C.M. three-momentum in MeV/c. The angle θ is the C.M. polar angle between q' and q in degrees, and φ is the azimuthal angle of the outgoing photon in degrees. Angles are shown for the in-plane, below-plane and above-plane OOPS's.

Electron Scattering Kinematics					In-plane		Below-plane		Above-plane	
E_i	E_f	θ_e	q	q'	θ	ϕ	θ	ϕ	θ	ϕ
568.3	493.7	25.77	237	43	108.6	180.0	123.9	62.4	123.9	297.6
610.4	510.8	24.52	240	65	90.0	180.0	90.0	90.0	90.0	270.0
632.4	511.6	23.64	240	84	90.0	180.0	90.0	90.0	90.0	270.0
651.2	512.3	22.76	240	100	90.0	180.0	90.0	90.0	90.0	270.0
669.2	513.0	21.82	240	115	90.0	180.0	90.0	90.0	90.0	270.0

TABLE 2. Systematic errors. The first column gives the final photon C.M. momentum. The second and third columns are the percent uncertainties for the OOPS tracking efficiencies, and the fourth column is the percent uncertainty in luminosity. The last two columns show the percent uncertainty in the Bethe-Heitler + Born cross section assuming ± 0.1 % uncertainty in the incident beam energy. The units of φ are degrees.

q' (MeV/c)	Oops Tracking Eff. Uncertainty (%)			Luminosity Uncertainty (%)			$d^5\sigma^{BH+Born}$ (%)	
	$\phi = 180$	$\phi = 90$	$\phi = 270$	$\phi = 180$	$\phi = 90$	$\phi = 270$	$\phi = 180$	$\phi = 90,270$
43	2.2	2.5	3.2	0.14	0.37	0.65	1.6	1.8
65	1.9	1.5	1.4	0.32			1.1	1.1
84	2.5	1.9	1.7	0.42			1.0	1.1
100	0.9	0.7	0.7	0.23			0.9	0.9
115	0.9	1.3	1.3	0.20			0.7	0.8

TABLE 3. VCS cross sections in units of $nb/\left(GeV \cdot sr^2\right)$. The errors are statistical and systematic, respectively. The units of φ are degrees.

q' (MeV/c)	$\phi = 180$	$\phi = 90$	$\phi = 270$
43	$5.73 \pm 0.29 \pm 0.16$	$10.68 \pm 0.50 \pm 0.33$	$11.48 \pm 0.64 \pm 0.42$
65	$2.19 \pm 0.18 \pm 0.05$	$5.53 \pm 0.18 \pm 0.10$	$5.34 \pm 0.21 \pm 0.10$
84	$1.61 \pm 0.13 \pm 0.04$	$3.95 \pm 0.17 \pm 0.09$	$3.95 \pm 0.14 \pm 0.08$
100	$1.16 \pm 0.06 \pm 0.02$	$2.86 \pm 0.07 \pm 0.04$	$2.87 \pm 0.08 \pm 0.04$
115	$0.99 \pm 0.05 \pm 0.01$	n/a	$2.32 \pm 0.16 \pm 0.04$

TABLE 4. Fitted values for Λ_α and Λ_β from VCS dispersion analyses in units of GeV. The errors shown for this experiment are statistical only; errors shown for the JLab I-a and I-b analyses are statistical and systematic, respectively.

Experiment	Λ_α	Λ_β
MIT-Bates	$0.60 \pm \begin{matrix} 0.17 \\ 0.11 \end{matrix}$	$0.51 \pm \begin{matrix} 0.39 \\ 0.15 \end{matrix}$
JLab I-a	$0.741 \pm 0.040 \pm 0.175$	$0.708 \pm 0.041 \pm 0.114$
JLab I-b	$0.702 \pm 0.035 \pm 0.037$	$0.632 \pm 0.036 \pm 0.023$

TABLE 5. Electric and magnetic mean square radii. The radii have unit of fm^2. The errors are statistical only.

	$\langle r_\alpha^2 \rangle$	$\langle r_\beta^2 \rangle$
Full Dispersion	$2.02^{+0.39}_{-0.59}$	$-4.67^{+5.36}_{-13.04}$
Asymptotic	$1.03^{+0.38}_{-0.58}$	$-8.42^{+6.17}_{-13.40}$
πN	0.99±0.05	3.76±1.65

TABLE 6. VCS response functions, polarizabilities, and electric polarizability mean square radius. The response functions have units of GeV^{-2}, polarizabilities have units of $10^{-4}\,fm^3$, and the mean square radius has units of fm^2. The errors are statistical and systematic, respectively.

Observable	LEX analysis	Dispersion analysis	HBCHPT [4]
$P_{LL} - P_{TT}/\varepsilon$	$54.5 \pm 4.8 \pm 3.4$	$46.7 \pm 4.9 \pm 3.4$	56.9
P_{LT}		$-8.9 \pm 4.2 \pm 1.4$	-6.5
$\alpha(Q^2 = 0.06)$		$7.85 \pm 0.87 \pm 0.60$	9.27
$\beta(Q^2 = 0.06)$		$2.69 \pm 1.48 \pm 0.49$	1.59
$\langle r_\alpha^2 \rangle$		$2.02^{+0.39}_{-0.59}$	1.7

Acknowledgements

The authors acknowledge and thank T. Hemmert, B. Holstein, B. Pasquini, and M. Vanderhaeghen for their comments and for communicating the results of their calculations. The authors also thank the staff of the MIT-Bates linear accelerator facility for their efforts on this experiment. This work was supported in part by D.O.E. grant DE-FG02-88ER40415.

References

[1] B. Holstein, Comm. Nuc. Part. Phys. **19**, 221 (1990).

[2] M. Schumacher, Prog. Part. and Nucl. Phys. **55**, 567 (2005).

[3] P.A.M. Guichon *et al.*, Nucl. Phys. A **591**, 606 (1995).

[4] T. R. Hemmert *et al.*, Phys. Rev. Lett. **79**, 22 (1997), and T.R. Hemmert *et al.*, Phys. Rev. D **62**, 014013 (2000).

[5] J. Roche *et al.*, Phys. Rev. Lett. **85**, 708 (2000).

[6] G. Laveissiere *et al.*, Phys. Rev. Lett. **93**, 122001 (2004).

[7] P. Bourgeois, *et al.*, Phys. Rev. Lett. **97**, 212001 (2006).

[8] P. Janssens, *et al.*, Eur.Phys.J., **A**37 (2008) 1.

[9] P.A.M. Guichon, and M. Vanderhaeghen, Prog. Part. Nucl. Phys. **41**, 125 (1998).

[10] S. Dolfini *et al.*, Nucl. Instum. Methods Phys. Res., Sect. A **344**, 571 (1994); J. Mandeville *et al.*, Nucl. Instrum. Methods Phys. Res., Sect. A **344**, 583 (1994) ; Z. Zhou *et al.*, Nucl. Instrum. Methods Phys. Res., Sect. A **487**, 365 (2002).

[11] X. Jiang, Ph.D. thesis, University of Massachusetts, 1998, unpublished.

[12] Fermi National Accelerator Labororatory report, NAL-64 (1978).

[13] H.W. Lewis, Phys. Rev. **78**, 526 (1950),

[14] M. Vanderhaeghen, *et al.*, Phys. Rev. C **62**, 025501 (2000).

[15] T. Zwart *et. al.*, Nucl. Instrum. Methods Phys. Res., Sect. A **384**, 299 (1997)

[16] G. Hoehler, E. Pietarinen, and I.Sabba-Stefanescu, Nuc. Phys. B **114**, 505 (1976).

[17] J. Friedrich and Th. Walcher, Eur. Phys. J. **A** 17, 607 (2003).

[18] B. Pasquini *et. al.*, Eur. Phys. J. A **11**, 185 (2001), and D. Drechsel, B. Pasquini, and M. Vanderhaeghen, Phys. Rep. 378, 99 (2003).

[19] D. Drechsel, O. Hanstein, S. S. Kamalov, and L. Tiator, Nucl. Phys **A** 645, 145 (1999).

[20] M. Gorchtein, C. Lorce, B. Pasquini, and M. Vanderhaeghen, Phys. Rev. Lett. 104, 112001 (2010).

[21] Private communication, H. Fonvieille.

[22] Private communication, B. Holstein.

[23] V. Bernard, N. Kaiser, A. Schmidt, and Ulf-G. Meiβner, Phys. Lett. **B** 319, 269 (1993), and V. Bernard, N. Kaiser, Ulf-G. Meiβner, and A. Schmidt, Z. Phys. **A** 348, 317 (1994).

[24] T. R. Hemmert, B. R. Holstein, G. Knochlein, and S. Scherer, Phys. Rev. D **55**, 2630 (1997).

[25] S. Eidelman *et al.*, Phys. Lett. B **592**, 1 (2004).

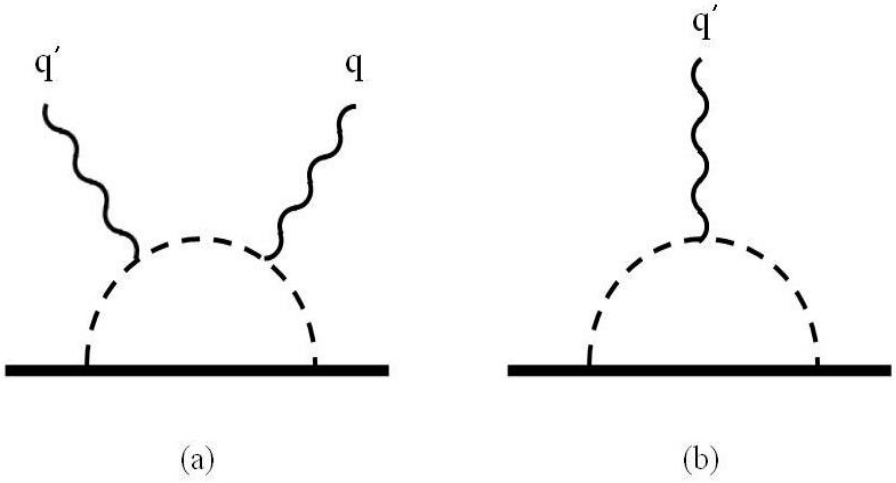

Fig.1. Dominant pion loop diagrams for (a) the proton polarizability, and (b) the proton electromagnetic form factor.

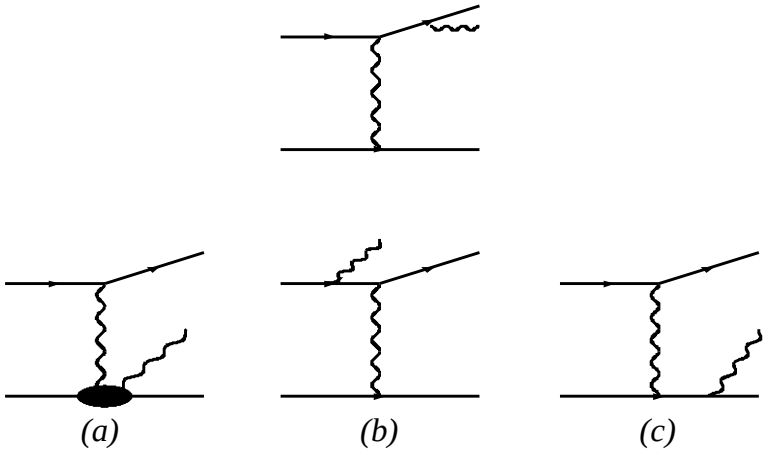

Fig. 2. Feynman diagrams for the VCS amplitude. Figure (a) shows the structure dependent, non-Born term, figure (b) the Bethe-Heitler amplitudes, and figure (c) the Born amplitude.

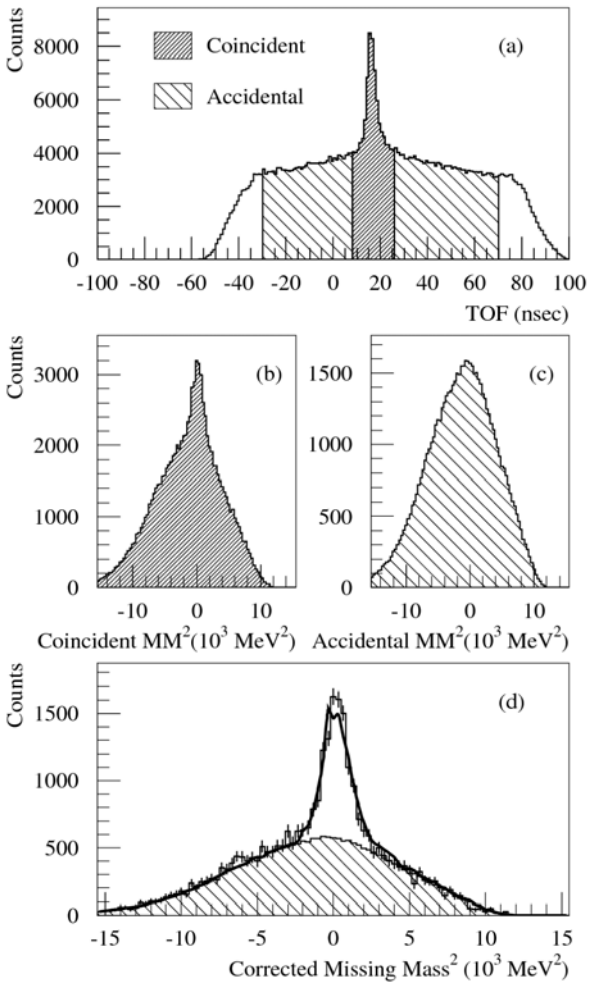

Fig. 3. Panel (a) shows the time-of-flight (TOF) distribution between the detected electron and proton. Panels (b) and (c) show the missing-mass squared (MM^2) distributions cut on the coincident peak and the accidental portions of the TOF distribution, respectively. Panel (d) shows the result of subtracting the distribution in panel (c) from the distribution in panel (b), where the weighting factor is given by the timing widths of the accidental and coincident TOF bins. The curves in panel (d) show peak and background fitting to the subtracted MM^2 distribution, as explained in the text.

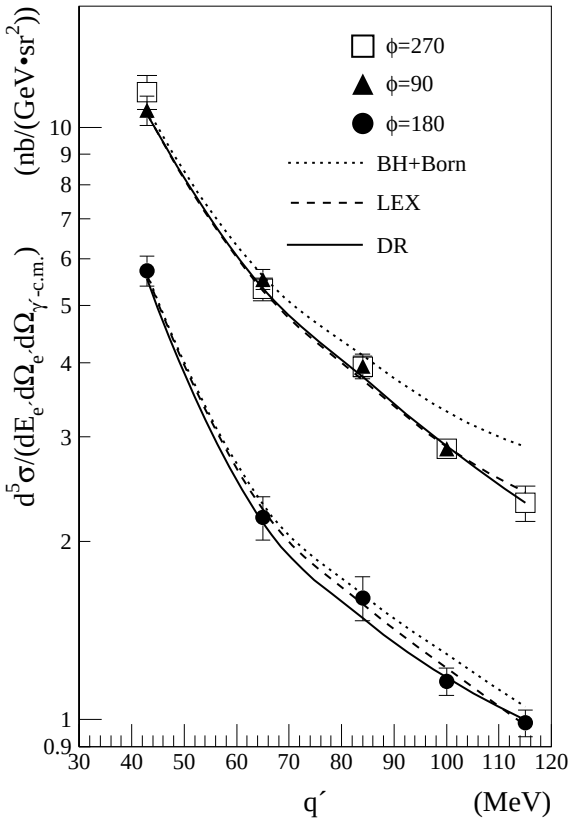

Fig. 4. VCS cross sections as a function of average q'. The dotted curves are Bethe-Heitler + Born, the dashed and solid curves are fits with LEX and dispersion analyses, respectively.

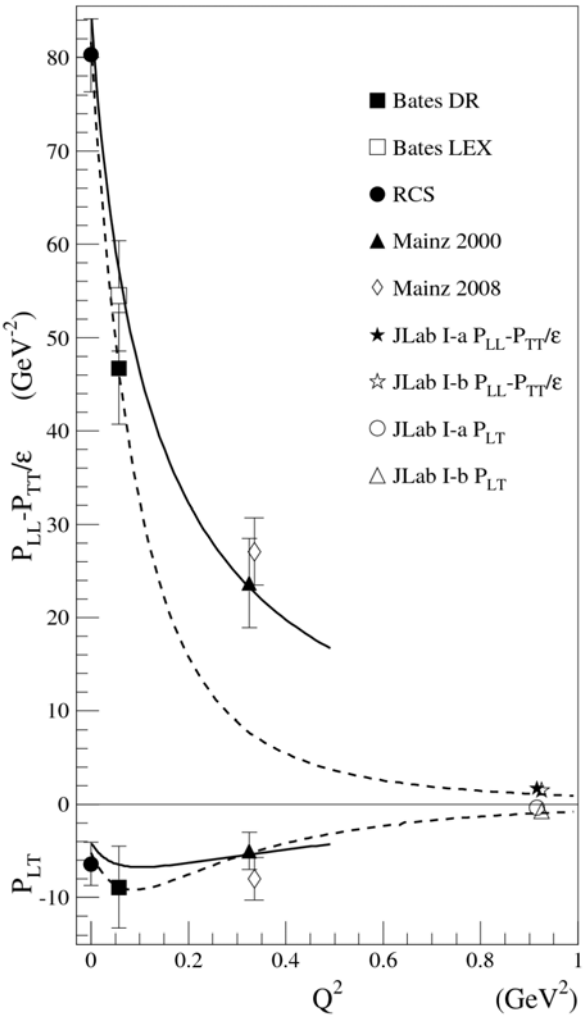

Fig. 5. VCS response functions from this experiment, RCS [2], Mainz 2000 [5], Mainz 2008 [8], and JLab [6]. The solid curves are $O(p^3)$ HBChPT [4] with $\varepsilon = 0.9$. The dashed curve is a dispersion model calculation that is fit to the RCS and MIT-Bates data points.

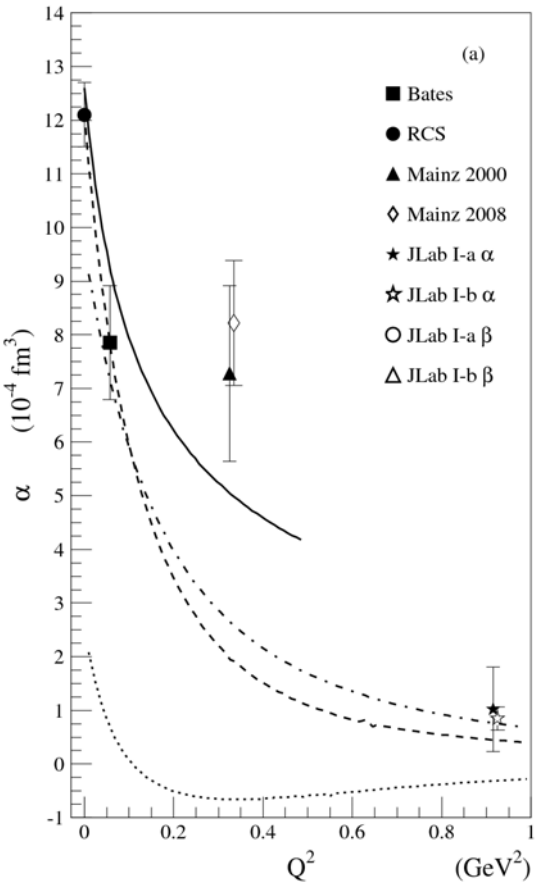
(a)
Bates
RCS
Mainz 2000
Mainz 2008
JLab I-a α
JLab I-b α
JLab I-a β
JLab I-b β
α (10^-4 fm^3)
Q^2 (GeV^2)
14
13
12
11
10
9
8
7
6
5
4
3
2
1
0
-1
0
0.2
0.4
0.6
0.8
1

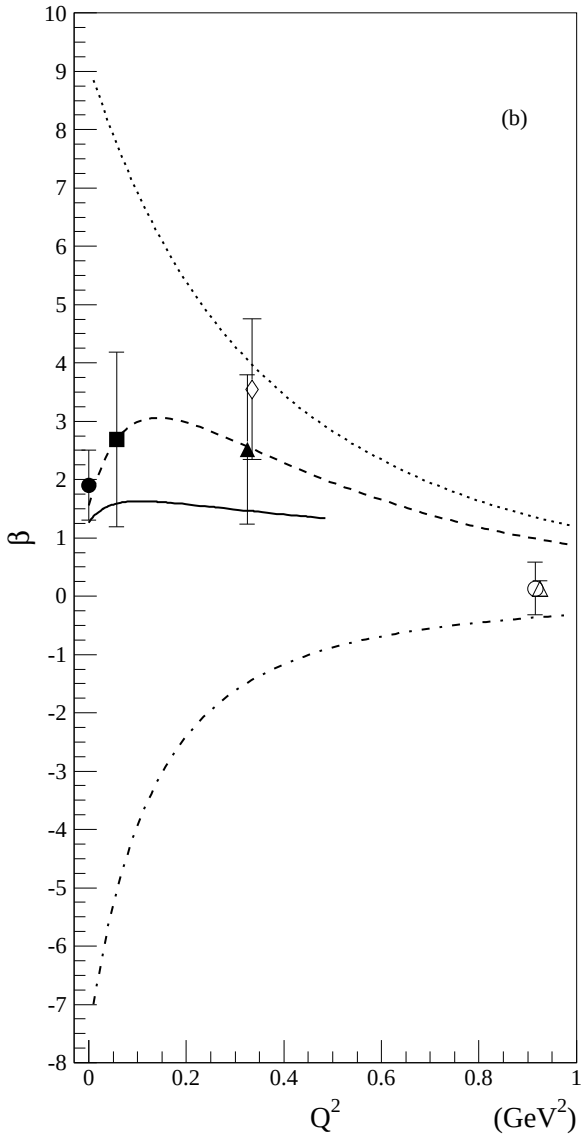

Fig. 6. Panels (a) and (b) show results for $\alpha(Q^2)$ and $\beta(Q^2)$, respectively. The references are the same as in Fig. 5 except for Mainz [20]. The solid curves are $O(p^3)$ HBChPT [4]. The dashed curve is the full dispersion calculation that is fit to the RCS and MIT-Bates data points. The dotted and dash-dotted curves are the πN and asymptotic contributions to the dispersion analysis fit, respectively.